

Assessment of the nutrient diol index (NDI) as a sea surface nutrient proxy using sinking particles in the East Sea

Jong-Ku Gal^{a,b}, Jung-Hyun Kim^{b,*}, Solbin Kim^a, Jeomshik Hwang^c, Kyung-Hoon Shin^{a,*}

^a Department of Marine Science and Convergence Technology, Hanyang University, 55 Hanyangdaehak-ro, Ansan 15588, Republic of Korea

^b Korea Polar Research Institute, 26 Songdomirae-ro, Incheon 21990, Republic of Korea

^c School of Earth and Environmental Sciences, Seoul National University, Seoul 08826, Republic of Korea

ARTICLE INFO

Keywords:

Nutrient diol index
Long chain diol
Paleo nutrient proxy
Sinking particle
East Sea

ABSTRACT

The Nutrient Diol Index (NDI) has been proposed as a paleo sea surface nutrient proxy. However, the NDI's broad applicability needs to be further assessed by examining its temporal variability in association with modern sea surface nutrient concentrations. This study is the first report to evaluate the NDI with respect to sinking particles in the East Sea. The NDI values showed seasonal variations resembling those of the surface phosphate concentrations in the study area. However, the calibration based on the sinking particles at 1000 m water depth ($NDI = 1.134 \times [PO_4^{4-}] + 0.115$, $R^2 = 0.59$, $n = 26$) deviated from the newly compiled global surface sediment dataset ($NDI = 0.392 \times [PO_4^{4-}] + 0.023$; $R^2 = 0.58$, $n = 566$). This local calibration predicted the phosphate concentrations in surface sediments in the East Sea better than the global calibration. Our study suggests that the difference of the calibration slope between the East Sea trap dataset and the global surface sediment dataset might be associated with different 1,14-diol producers and their sensitivity to nutrient concentrations in the East Sea. Accordingly, the NDI should be further assessed in various oceanic settings before it is routinely used to reconstruct sea surface nutrient conditions.

1. Introduction

Nutrients in sea surface mixed layers are one of the key environmental factors controlling primary productivity (e.g., Behrenfeld et al., 2006). Thus, paleonutrient records are needed to obtain information on past primary production (e.g., Marchitto, 2013). Recently, long chain diols (LCDs) composed of long alkyl chains (≥ 28 C atoms) with alcohol groups at C₁ and a mid-chain position (e.g., carbon numbers 13, 14, and 15) have been used to develop a quantitative paleo sea surface nutrient proxy based on the global surface sediment dataset (Gal et al., 2018). The resulting Nutrient Diol Index (NDI) is a LCD ratio using the C₂₈ 1,14-diol and the C_{28:1} 1,14-diol in the numerator and the 1,13-, 1,14-, and 1,15-diols (excluding the C₃₂ 1,15-diol) in the denominator, showing positive correlations between NDI values and sea surface phosphate and nitrate concentrations.

Thus far, this NDI has been applied to two sediment cores to assess its applicability in the East Sea (Gal et al., 2019) and the eastern South Pacific (de Bar et al., 2018). The NDI-derived phosphate and nitrate concentrations for the core-top sediment in the East Sea were within the average ranges for the last ~20 years at the study site. The down-core

NDI record showed higher surface nutrient conditions between 1884 CE and 1911 CE, which might be associated with stronger upwelling intensity, supporting the use of the NDI as a past sea surface nutrient proxy. However, the NDI-derived nutrient concentrations were lower in the Chile-Peru margin in the eastern south Pacific during the intensified upwelling interval (de Bar et al., 2018). Thus, the authors argued that the NDI should be considered as an indicator for the *Proboscica* productivity rather than for the surface nutrient condition. Accordingly, more works are needed to evaluate the applicability of the NDI in various oceanic settings, especially by examining its temporal variability in association with modern sea surface nutrient concentrations.

In this study, we analyzed the LCDs of sinking particles collected over a year ($n = 46$) and core-top sediments ($n = 4$) collected from the East Sea. We examined the temporal variation for individual LCD fluxes to understand their biological sources and transport processes to the sea floor. We also examined the NDI's seasonal variability in association with sea surface nutrient concentrations derived from the World Ocean Atlas 13 (WOA13) dataset (Garcia et al., 2013a) and assessed the NDI as a paleo sea surface nutrient proxy to reconstruct changes in sea surface phosphate (or nitrate) concentrations.

* Corresponding authors.

E-mail addresses: jhkim123@kopri.re.kr (J.-H. Kim), shinkh@hanyang.ac.kr (K.-H. Shin).

<https://doi.org/10.1016/j.marchem.2021.103937>

Received 7 September 2020; Received in revised form 31 December 2020; Accepted 22 January 2021

Available online 6 February 2021

0304-4203/© 2021 Elsevier B.V. All rights reserved.

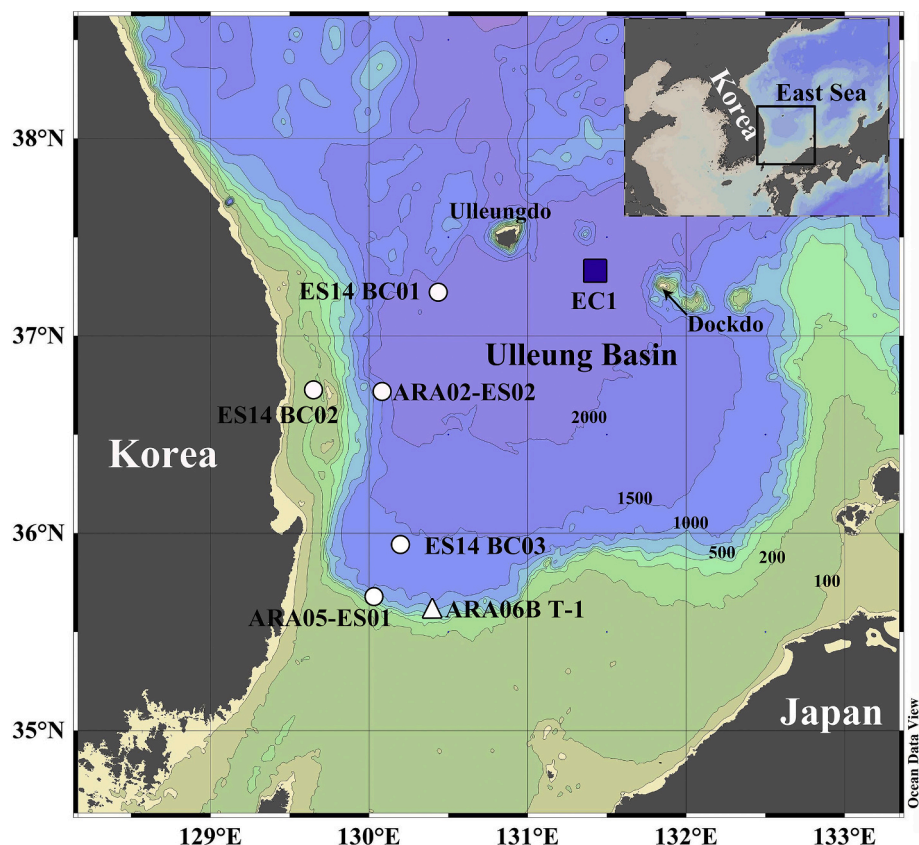


Fig. 1. A map of study area with the sampling locations. The triangle represents the sediment trap mooring station (EC1). The open circles and the triangle represent the surface sediment and suspended particulate matter (SPM) sampling locations, respectively. See details in Table 1.

2. Materials and methods

2.1. Sample collection

Sinking particles were collected using two sediment traps on a mooring in the Ulleung Basin (EC1: 37.33N, 131.45E) in the southwestern part of the East Sea (Fig. 1). The sediment trap mooring array and sample collection were described in detail in Kim et al. (2017). The sediment traps were deployed at 1040 m (hereafter 1000 m nominal depth) and 2280 m (hereafter 2300 m nominal depth) water depths and sinking particles were collected at 10 to 15 day sampling intervals between 15 March 2011 and 16 February 2012.

Core-top sediment samples were collected using a box corer and a

multi-corer aboard the R/V Araon (Table 1). Subcore samples were collected using acrylic barrels from the box core canister. Sediment cores were sliced at 1 cm or 2 cm thicknesses and stored in pre-combusted glass jars. Core-top samples were stored at -20°C until analysis. Sediment samples were freeze-dried and homogenized using mortar and pestle.

2.2. Biomarker analysis

The sediment trap and core-top sediment samples were ultrasonically extracted using a solvent mixture of 2:1 (v:v) dichloromethane (DCM) to methanol (MeOH). The total extract was separated into three fractions using an aluminum oxide column. The purification of the total lipid extract and the gas chromatography analysis were performed as

Table 1

NDI values and estimated phosphate concentrations from suspended particulate matter (SPM), surface sediments, and sinking particles in the East Sea. Annual mean phosphate concentrations were obtained from the WOA13 (Garcia et al., 2013a). A newly established NDI global calibration and a local East Sea calibration are shown in the text.

Sample name	Sample type	Latitude (N)	Longitude (E)	Annual mean phosphate concentration (μM)	NDI	NDI-derived phosphate (μM)		Reference
						Global calibration	East Sea calibration	
ARA06A-T1 surface	SPM	35.558	130.417	0.18	0.345	0.82	0.20	Gal et al., 2018
ES14 BC03 0–1 cm	Sediment	35.911	130.211	0.24	0.299	0.71	0.16	Gal et al., 2019
ES14 BC01 0–1 cm	Sediment	37.201	130.418	0.25	0.404	0.97	0.26	this study
ES14 BC02 0–1 cm	Sediment	36.701	129.656	0.49	0.427	1.03	0.28	this study
ARA05-ES01 MUC 0–2 cm	Sediment	35.644	130.031	0.24	0.323	0.76	0.18	this study
ARA02-ES02 MUC 2–4 cm	Sediment	36.685	130.092	0.25	0.352	0.84	0.21	this study
EC1 1000 m	Sinking particle	37.326	131.450	0.25	0.338*	0.80	0.20	this study
EC1 2300 m	Sinking particle	37.326	131.450	0.25	0.341*	0.81	0.20	this study

* Flux weighted values.

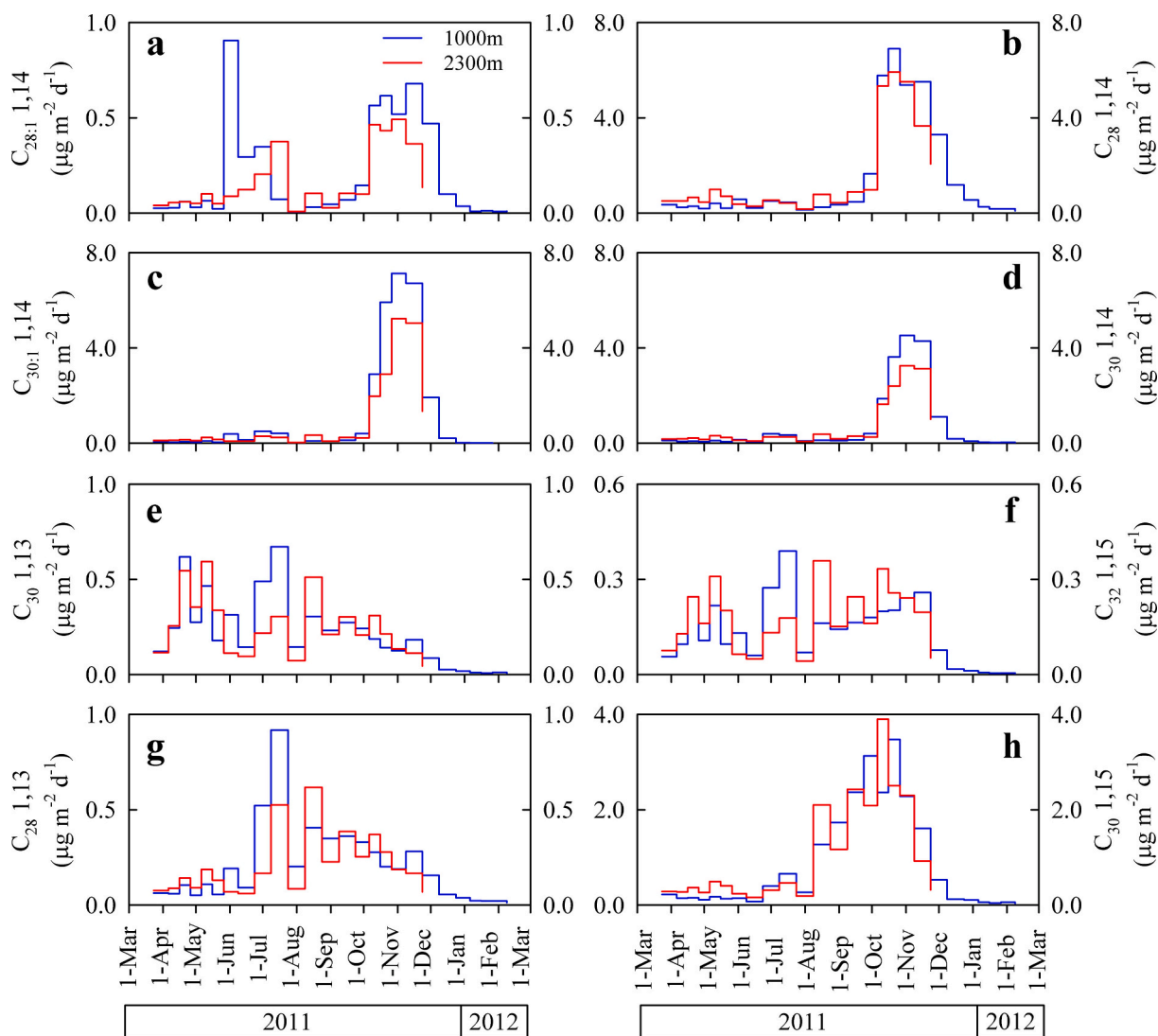


Fig. 2. Temporal variation in sinking particle LCD (a–h) fluxes collected at 1000 m (blue line) and 2300 m (red line) water depths. See details in Table S1. (For interpretation of the references to colour in this figure legend, the reader is referred to the web version of this article.)

previously described (Gal et al., 2018). In brief, the fraction of DCM: MeOH (1,1, v,v) was silylated with *N,O*-bis(trimethylsilyl)tri-fluoroacetamide (BSTFA) and pyridine. The LCDs were analyzed using gas chromatograph (Agilent 7820A) coupled to mass spectrometer (Agilent 5977E MSD) and equipped with a fused silica capillary column (Agilent HP-5 ms, 30 m length, 0.25 mm i.d., 0.25 µm thickness). The LCDs were identified and quantified using the full scan mode (m/z 50–800) and the selected ion monitoring (SIM) mode as described by Rampen et al. (2008, 2009). Our in-house standard sediments were analyzed every 10 samples to calculate replicate NDI analytical errors (cf. Gal et al., 2017). NDI's standard deviation was ± 0.02 ($n = 7$).

2.3. Nutrient data and statistical analysis

The monthly sea surface phosphate and nitrate concentration data were obtained from the WOA13 one-degree climatological dataset (37.5N, 131.5E, Garcia et al., 2013a). The measured surface phosphate and nitrate concentration data with a two-month interval were acquired from the Korea Oceanographic Data Center (KODC) of the National Institute of Fisheries Science (line 105, site number 11; 37.55N, 131.24E; <http://www.nifs.go.kr>).

All statistical analyses were performed using the R program (R Core Team, 2015). The Pearson correlation coefficients between the

fractional abundances of the LCDs and the environmental data were determined using the Vegan package (Oksanen et al., 2013). Principle component analysis (PCA) was conducted with the FactoMineR package (Lê et al., 2008). The PCA was performed on the fractional abundances of the 1,13-, 1,14-, and 1,15-diols, and the environmental parameters such as sea surface temperature (Locarnini et al., 2013), salinity (Zweng et al., 2013), and phosphate and nitrate concentrations extracted from the WOA13 (Garcia et al., 2013a). Analysis of covariance (ANCOVA) was also performed to obtain multiple linear regressions and to compare the regression slopes of the NDI calibrations.

3. Results

3.1. Seasonal flux of LCDs

The total LCD fluxes in the upper (1000 m water depth) and lower (2300 m water depth) sediment traps ranged from 0.16 to $21.08 \mu\text{g m}^{-2} \text{d}^{-1}$ (average $4.68 \pm 6.49 \mu\text{g m}^{-2} \text{d}^{-1}$) and from 0.65 to $17.35 \mu\text{g m}^{-2} \text{d}^{-1}$ (average $5.10 \pm 5.31 \mu\text{g m}^{-2} \text{d}^{-1}$), respectively (Supplementary Table S1). The $C_{28:1}$ 1,14-diol showed the highest fluxes in late spring (21 May–1 July) and late fall (16 September–16 December) (Fig. 2a). The C_{28} 1,14-diol flux showed an increase in late fall (16 September–1 January), but did not increase in late spring (Fig. 2b). Both saturated and

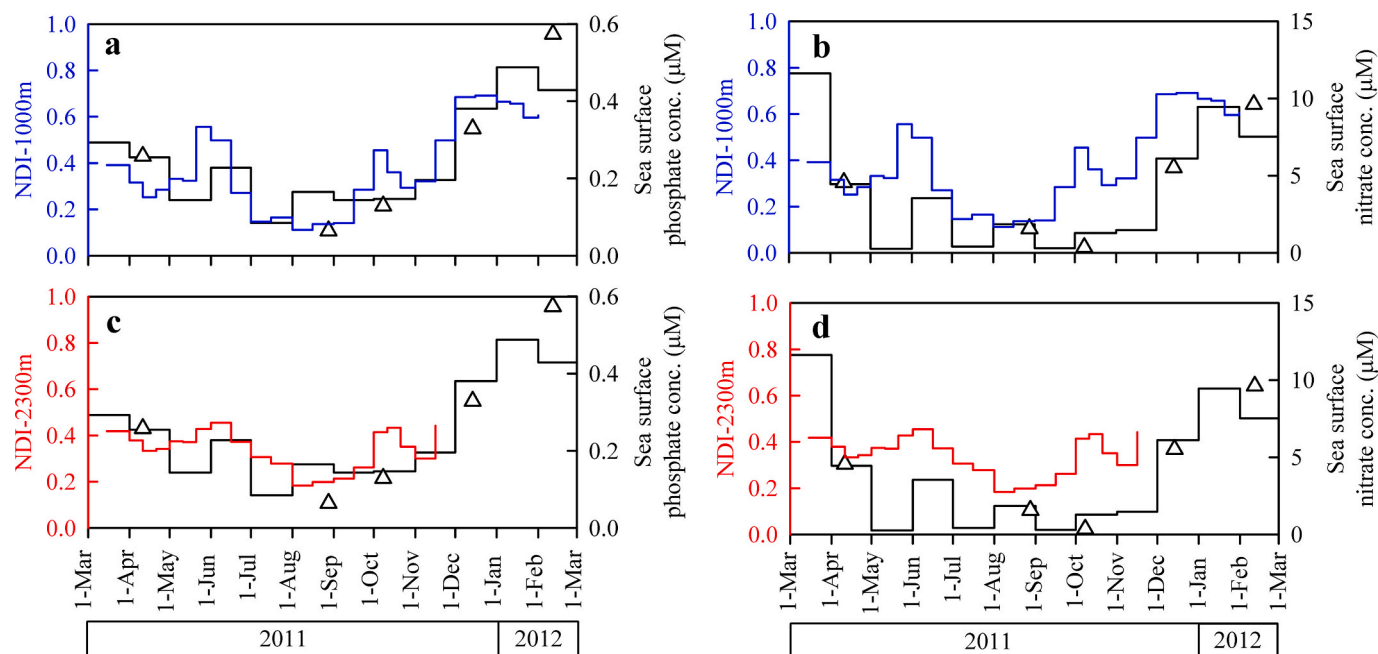


Fig. 3. NDI values of the sinking particles at 1000 m (blue line: a and b) and 2000 m (red line: c and d) water depths in the East Sea. Monthly sea surface phosphate (a and c) and nitrate (b and d) concentrations are represented by black lines. Nutrient data were obtained from the World Ocean Atlas 13 one-degree climatological dataset (37.5N, 131.5E, Garcia et al., 2013a). The surface nutrient concentration data (open triangle) were obtained from the Korea Oceanographic Data Center (KODC) of National Institute of Fisheries Science, South Korea (line 105, site number 11; 37.55N, 131.24E, www.nifs.go.kr). (For interpretation of the references to colour in this figure legend, the reader is referred to the web version of this article.)

unsaturated C_{30} 1,14-diol fluxes increased in late fall (1 October–1 December) (Fig. 2c–d) with slightly shorter periods than the saturated and unsaturated C_{28} 1,14-diols (16 September–16 December). The 1,13- and 1,15-diol fluxes were generally lower than the 1,14-diol fluxes except in the spring (11 April–21 May) and summer (1 July–1 October) (Fig. 2e–h). The C_{28} and C_{30} 1,13-diol and C_{32} 1,15-diol fluxes were highest between 1 and 16 July. The C_{30} 1,13-diol fluxes correlated positively with the C_{32} 1,15-diol at 1000 m and 2300 m water depths ($R^2 = 0.63$, $n = 46$, $p < 0.001$, data not shown). The average fluxes of the 1,13- and 1,15-diols were 1.37 ± 1.27 and $1.70 \pm 1.31 \mu\text{g m}^{-2} \text{d}^{-1}$ in the upper and lower sediment traps, respectively. The average fluxes of all of the 1,14-diols were 3.31 ± 5.66 and $3.40 \pm 4.54 \mu\text{g m}^{-2} \text{d}^{-1}$ in the upper and lower sediment traps, which accounted for 71% and 67% of the total fluxes of the LCDs in the upper and lower sediment traps, respectively.

3.2. Seasonal variation of the NDI

Mean NDI values at 1000 m and 2300 m water depths were 0.386 ± 0.186 (ranging from 0.111 to 0.691) and 0.343 ± 0.083 (ranging from 0.184 to 0.455), respectively (Fig. 3, Supplementary Table S1). The flux weighted NDI values at 1000 m and 2300 m water depths were 0.338 and 0.341, respectively (Table 1). The NDI values decreased in summer and increased in winter; the highest NDI value occurred in winter (16 December–1 January), and the lowest NDI value in summer (1–16 August) at 1000 m water depth. Temporally, the NDI increased in early summer (21 May–16 June) at 1000 m water depth. We measured the highest NDI value at 2300 m water depth in early summer (1–16 June) due to insufficient winter samples at that depth. However, the lowest NDI value at 2300 m water depth corresponded with the same time period at 1000 m water depth.

4. Discussion

4.1. Biological sources of LCDs

Proboscia diatoms are considered to be the main producers of

saturated and unsaturated C_{28} and C_{30} 1,14-diols (Sinninghe Damsté et al., 2003; Rampen et al., 2007). The average flux of all of the 1,14-diols accounted for more than 67% of the total LCDs in the East Sea, indicating that *Proboscia* diatoms played an important role as a biological producer of the LCDs in the East Sea. Interestingly, the fluxes of each 1,14-diol slightly differed from each other depending on seasons (Fig. 2a–d). This is probably due to seasonal variations in *Proboscia* communities, producing different types of the LCDs. In a culture experiment, *P. alata* produced the $C_{28:1}$ 1,14-diol, which accounted for 90% of the 1,14-diols while *P. inermis* produced both saturated and unsaturated C_{28} 1,14-diols (Sinninghe Damsté et al., 2003; Rampen et al., 2007). Hence, it appears that the increasing fluxes of the $C_{28:1}$ 1,14-diol during the summer were associated with the predominance of *P. alata* during the summer in the eastern coastal areas of Korea (Kang et al., 2003, 2005). In contrast, the increasing fluxes of all of the 1,14-diols in winter might be related to *P. indica* which can also produce all these compounds (Sinninghe Damsté et al., 2003; Rampen et al., 2007, 2009). *P. indica* has been reported in June, September, and October in the Yellow Sea, the Korea Strait, and the eastern coastal areas of Korea (Yun and Lee, 2011; Lee et al., 2015; Yoon, 2017). However, it is still unknown whether this species primarily occurs in the study area.

The C_{30} 1,13-diol and C_{32} 1,15-diol fluxes showed similar temporal variations at 1000 m and 2300 m water depths (Fig. 2e–f), suggesting similar biological sources during the sampling period. The C_{28} – C_{32} 1,13- and 1,15-diols are produced by Eustigmatophyceae in both freshwater and marine environments (Volkman et al., 1992; Gelin et al., 1997; Méjanelle et al., 2003; Shimokawara et al., 2010). Recently, the C_{32} 1,15-diol was proposed as a riverine input tracer (Versteegh et al., 1997; de Bar et al., 2016; Lattaud et al., 2017a, 2017b, 2018). Hence, the C_{30} 1,13-diol and the C_{32} 1,15-diol could be associated with riverine sources. In our study area, there are no large rivers draining directly into the Ulleung Basin in the East Sea. Therefore, marine production is more likely the major biological sources of the C_{30} 1,13-diol and the C_{32} 1,15-diol in our study area. However, we should further explore the possibility of the riverine inputs of the C_{30} 1,13-diol and the C_{32} 1,15-diol,

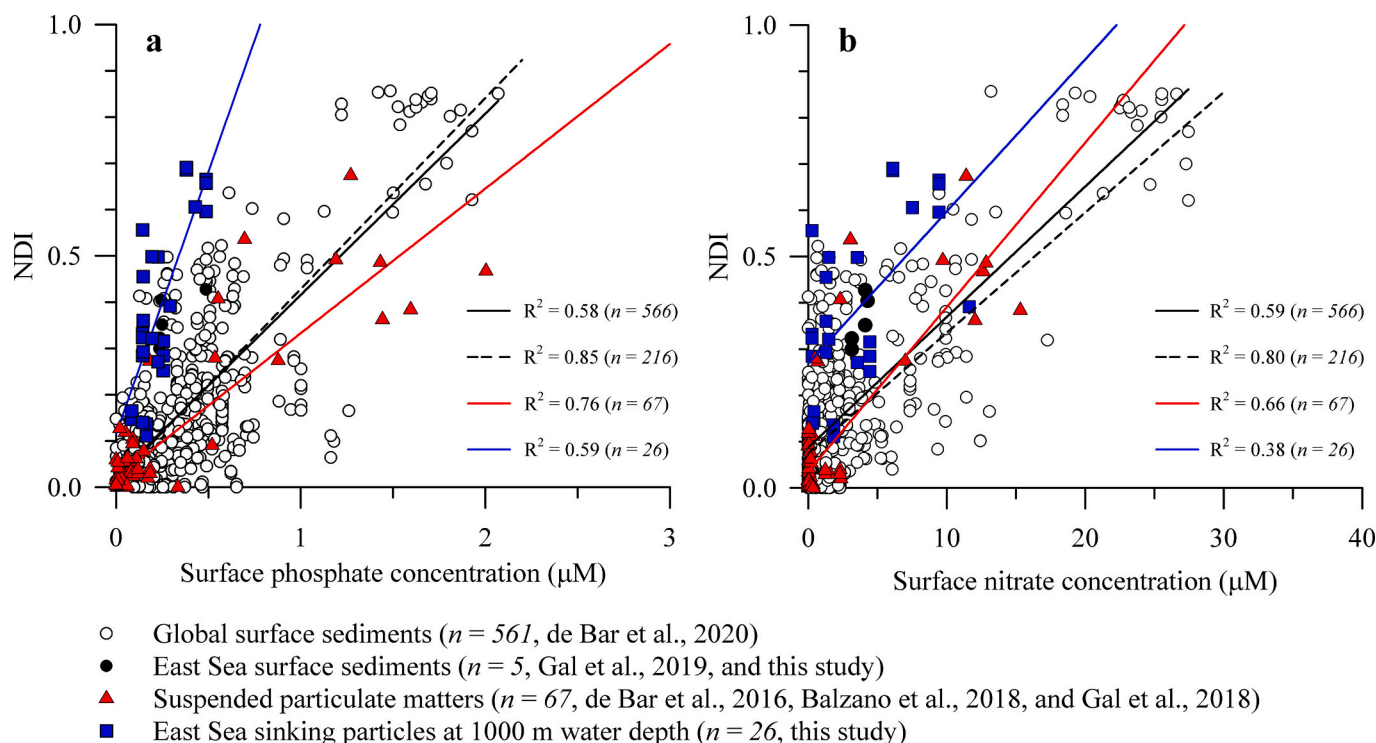


Fig. 4. Scatter plots of nutrient concentrations and NDI values. Annual mean and monthly mean nutrient concentrations are from the WOA13 for the surface sediments and the sinking particles. Black solid lines represent global correlations for the newly compiled global surface sediment dataset ($n = 566$) and black dashed lines indicate the initial global correlations ($n = 216$) previously suggested by Gal et al. (2018). Blue and red solid lines represent linear correlations for the suspended particulate matter ($n = 67$) and the sinking particles at 1000 m water depth in the East Sea ($n = 26$), respectively. (For interpretation of the references to colour in this figure legend, the reader is referred to the web version of this article.)

considering that one of the largest rivers in the world, the Changjiang River (Yangtze River) is flowing into the East China Sea which water mass is being further transported to the East Sea via the Kuroshio Current (Ichikawa and Beardsley, 2002).

Compounds such as the C_{28} and C_{30} 1,13-diols and the C_{30} and C_{32} 1,15-diols, which originate from Eustigmatophyceae, showed higher fluxes at 2300 m water depth than at 1000 m water depth (Fig. 2e–h). Eustigmatophyceae are photosynthetic autotrophs, thus mostly inhabiting the surface layers in marine environments. Therefore, this mismatch of LCD fluxes between the upper and lower traps provides a hint that lateral transport, probably in part associated with sediment resuspension in the shelf and slope regions of the Ulleung Basin (e.g., Kim et al., 2017), played a role in LCD inputs to the deeper water depth in the study area. Consequently, lateral transport of the LCDs might have influenced the NDI more strongly at 2300 m water depth than at 1000 m water depth. However, the annual flux weighted NDI values were similar between 1000 m (0.338) and 2300 m (0.341) water depths (Table 1), falling within the NDI calibration error range (± 0.14 for the NDI; Gal et al., 2018). Therefore, the lateral transport effect on the NDI seems to be negligible in the study area, which is probably due to comparable NDI values of resuspended shelf/slope sediments to those of the epipelagic zone in the Ulleung Basin. Nonetheless, this possible effect on the NDI should be further explored based on the extended dataset

covering broader shelf-slope-basin areas.

4.2. Environmental factors affecting the LCD distribution

To explore the potential environmental factors which influence the LCD distribution, we first compared the WOA13 data (Garcia et al., 2013a) with the KODC data (<http://kodc.nifs.go.kr>). Little differences were observed for the study period (Fig. 3), indicating that the WOA13 data reflect well temporal variation at the study site. The NDI variations were similar at 1000 m and 2300 m water depths (Fig. 3), although winter signals were missing at 2300 m water depth because of the low mass fluxes and a low trapping efficiency for this period (Kim et al., 2017). Interestingly, the NDI values at 1000 m water depth mimicked the temporal nutrient concentration (phosphate and nitrate) variation with a declining trend in summer and an increasing trend in winter. The NDI at 1000 m water depth correlated better with phosphate concentrations ($R^2 = 0.59$, $n = 26$) than nitrate concentrations ($R^2 = 0.38$, $n = 26$) (Fig. 4). This is consistent with a previous study based on a global surface sediment dataset (Gal et al., 2018). Therefore, phosphate concentrations are a major environmental factor for the NDI, influencing the production of the saturated and unsaturated C_{28} 1,14-diols in the East Sea.

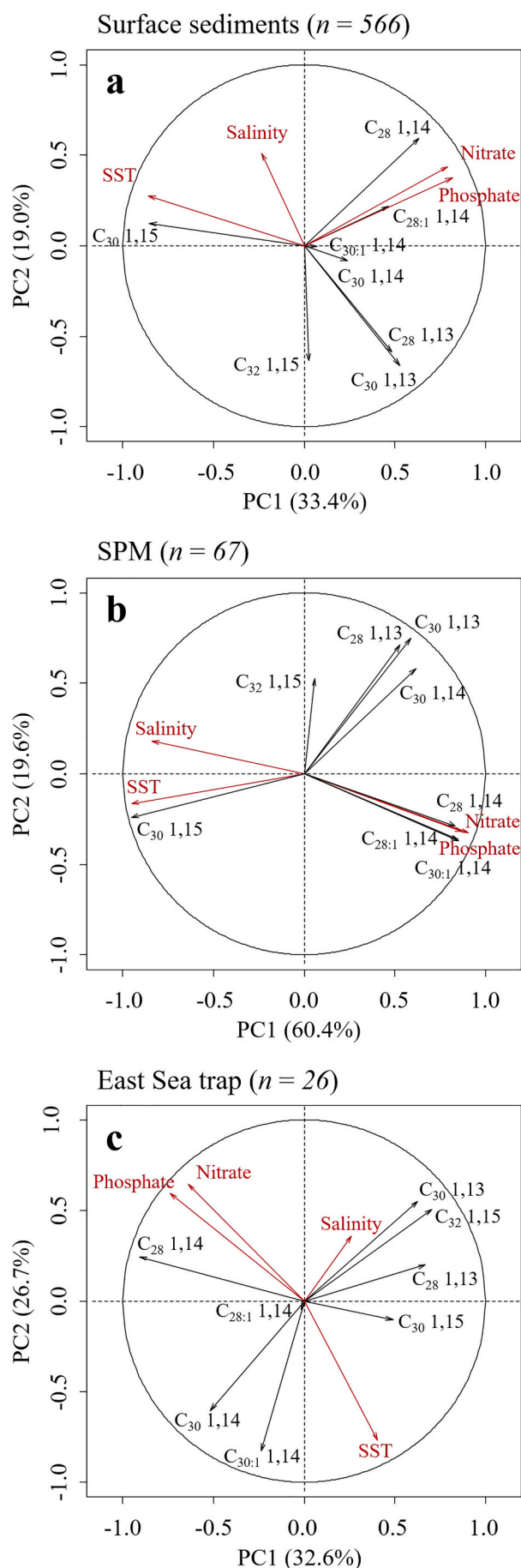
Recently, de Bar et al. (2020) compiled LCD data from 595

Table 2

Pearson correlation coefficients between the fractional abundances of the LCDs from the global sea surface sediment dataset ($n = 566$) and the sea surface environmental data from the WOA13 (Garcia et al., 2013a).

	C_{28} 1,14	$C_{28:1}$ 1,14	C_{30} 1,14	$C_{30:1}$ 1,14	C_{28} 1,13	C_{30} 1,13	C_{30} 1,15	C_{32} 1,15
Phosphate	<u>0.73</u>	0.40	0.01	0.00	0.12	0.22	<u>-0.56</u>	-0.07
Nitrate	<u>0.73</u>	0.45	-0.04	-0.04	0.11	0.17	<u>-0.48</u>	-0.13
Salinity	0.07	-0.07	0.13	-0.21	-0.13	-0.31	0.19	-0.43
Temperature	-0.33	-0.27	-0.37	-0.10	<u>-0.56</u>	<u>-0.55</u>	<u>0.77</u>	-0.08

Significant correlations (p value < 0.01) are indicated in bold, and underlined for $r \geq 0.5$ and $r \leq -0.5$.



(caption on next column)

Fig. 5. PCA biplots of the fractional abundances of the LCDs and environmental parameters based on (a) the global sea surface sediment dataset ($n = 566$, Gal et al., 2019, de Bar et al., 2020, and this study), excluding unavailable and co-eluted compounds data, (b) the sinking particle dataset at 1000 m water depth in the East Sea ($n = 26$, this study), and (c) the suspended particulate matter dataset ($n = 67$, de Bar et al., 2016, Balzano et al., 2018, and Gal et al., 2018). Black and red lines indicate the loading of 1,14-diols and environmental factors, respectively. Annual mean SST, salinity, phosphate, and nitrate data were from the WOA13 for the global sediment dataset. For the sinking particles, SST data were obtained from the satellite AVHRR daily data (NOAA, <http://www.esrl.noaa.gov>), salinity data from the moored sensor in the East Sea, and phosphate and nitrate data from the WOA13. (For interpretation of the references to colour in this figure legend, the reader is referred to the web version of this article.)

worldwide surface sediments to re-calibrate the Long-chain Diol Index (LDI) as a paleo-temperature proxy (Rampen et al., 2012). For this study, we excluded 34 data points from the de Bar dataset because individual LCD data were not available or some LCDs co-eluted with other compounds. We included five data points from the East Sea (Table 1). Consequently, the newly compiled global surface sediment dataset is composed of 566 data points (Fig. 4). The Pearson correlation showed that the C_{28} 1,14-diol from this new global surface sediment dataset was positively correlated with the phosphate and nitrate concentrations (Table 2). The $C_{28:1}$ 1,14-diol also had a significant correlation with nutrients, but the correlation coefficient values were slightly lower than those of the C_{28} 1,14-diol. In contrast, the correlation between the C_{30} 1,15-diol and nutrients was negative, whereas the C_{30} and $C_{30:1}$ 1,14-diols showed very weak correlations with nutrients (p value > 0.1). These results are in good agreement with the previous study (Gal et al., 2018), confirming that only the saturated and unsaturated C_{28} 1,14-diols were strongly associated with the phosphate and nitrate concentrations.

To further assess the relationships between the LCDs and the environmental data (cf. Gal et al., 2018), we performed PCA using the newly compiled surface sediment dataset ($n = 566$). The first two PCA components explained a cumulative 52.4% of the variance (Fig. 5a). The saturated and unsaturated C_{28} 1,14-diols were positively loaded on the first principal component, along with sea surface nutrient concentrations (PC1, 33.4% of the variance). In general, these results are in good agreement with the previous study, which also used the surface sediment dataset ($n = 216$, Gal et al., 2018). However, it should be noted that the positive loadings of the saturated and unsaturated C_{30} 1,14-diols on the PC1 were much weaker than those of the C_{28} and $C_{28:1}$ 1,14-diols and the C_{30} 1,15-diol was negatively loaded together with sea surface temperature on the PC1. It is also worthwhile to note that the C_{30} 1,13-diol and the C_{32} 1,15-diol were negatively loaded opposite to salinity on the second principal component (PC2, 19.0% of the variance).

We also analyzed the newly compiled suspended particulate matter (SPM) dataset ($n = 67$) for PCA (Fig. 5b). Similar to the global surface sediment dataset (see Fig. 5a), the saturated and unsaturated C_{28} 1,14-diols were positively loaded together with nutrients on the PC1 (60.4% of the variance). The C_{32} 1,15-diol was positively loaded on PC2 (19.6% of the variance) apart from other compounds. Interestingly, the positive loading of the $C_{30:1}$ 1,14-diol with nutrients was stronger in the SPM dataset than in the global surface sediment dataset. A previous study examined the oxic degradation effect on the LCDs based on the surface sediments collected from different oxygen concentrations of the water column in the northern Arabian Sea (Rodrigo-Gámiz et al., 2016). That study showed that the ratio of $C_{30:1}/C_{30}$ 1,14-diol rapidly decreased with water depth, while the ratio of $C_{28:1}/C_{28}$ 1,14-diol remained more or less constant (see Supplementary Fig. S1). The authors thus suggested that the $C_{30:1}$ 1,14-diol was more susceptible to oxic degradation than the $C_{28:1}$ 1,14-diol. Accordingly, our PCA results suggest that the $C_{30:1}$ 1,14-diol of the SPM was less subject to oxic degradation than that of the

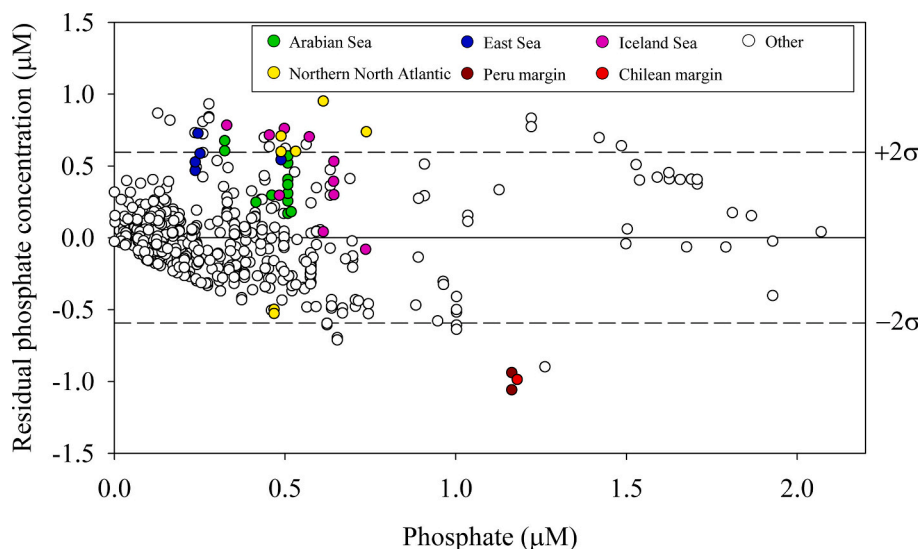


Fig. 6. Residual phosphate concentrations for the global sea surface sediment dataset ($n = 566$). Annual mean phosphate concentrations were obtained from the WOA13. The residual phosphate concentrations were estimated by subtracting the WOA13-derived phosphate concentrations from the NDI-derived phosphate concentrations using a newly established global calibration in this study (see Fig. 4a). Solid and dashed lines denote the mean and standard deviation (two-sigma, $\pm 2\sigma$) of the residual concentrations.

global surface sediment dataset. This might be associated with shorter oxic exposure time of the SPM than the surface sediments.

In order to assess whether the relationship between the LCDs and the environmental parameters observed in the global surface sediment dataset can be traced to sinking particles, we also performed PCA using the trap dataset ($n = 26$) obtained from 1000 m water depth (Fig. 5c). The C_{28} 1,14-diol was negatively plotted together with nutrients on the PC1 (32.6% of the variance), but the loading of the $C_{28:1}$ 1,14-diol was very weak. The saturated and unsaturated C_{30} 1,14-diols were negatively loaded with sea surface temperature on the PC2 (26.7% of the variance). Notably, the C_{30} 1,13-diol and the C_{32} 1,15-diol were positively loaded together with salinity on PC1, which was opposite to the relationship observed in the global surface sediment dataset (Fig. 5a). This PCA result hints that the C_{30} 1,13-diol and the C_{32} 1,15-diol in the study area could be, albeit minor, influenced by riverine inputs, probably from large Chinese and small Korean rivers flowing into the East China Sea which water mass is being further transported to the East Sea via the Kuroshio Current (Ichikawa and Beardsley, 2002).

4.3. Global vs. regional NDI calibrations

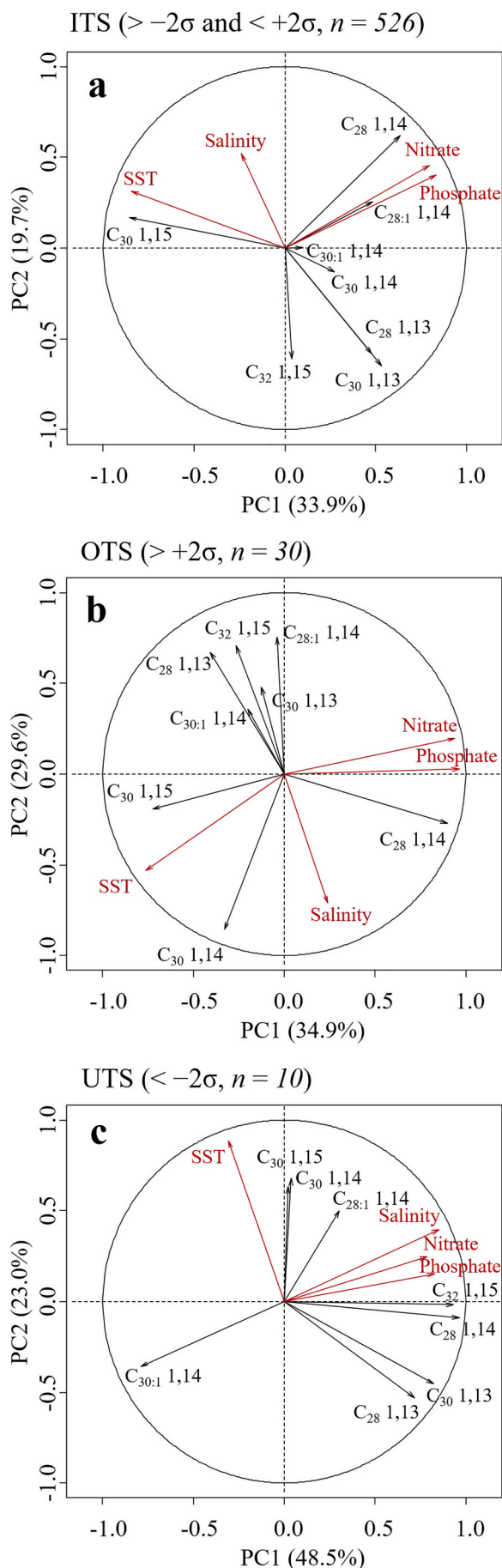
In order to assess the previous calibration between the NDI and phosphate in surface sediments (Gal et al., 2018), we examined the relationship using the newly compiled global surface sediment dataset ($n = 566$). The regression slope of the new global calibration ($\text{NDI} = 0.392 \times [\text{PO}_4^{4-}] + 0.023$, $R^2 = 0.58$, $n = 566$, $p < 0.0001$, Fig. 4a) was not statistically different (ANCOVA, $F_{(1,778)} = 0.03$, $p = 0.87$) from the previous calibration (Gal et al., 2018). However, the correlation coefficient of the new calibration for phosphate (0.58) was lower than that of the previous calibration (0.85). It is possible that some of the nutrient data were inaccurate since the WOA13 only had a one-degree resolution, which cannot adequately cover the NDI data. It could also be due to the narrow nutrient concentration range of the calibration dataset. For example, the NDI data corresponding to surface phosphate concentrations less than $1 \mu\text{M}$ accounted for 94% ($n = 532$) of the total number ($n = 566$). Furthermore, we found that some samples, especially from marginal seas and high latitude areas, showed large differences between the WOA13- and NDI-derived phosphate concentrations (Fig. 6, see also Supplementary Fig. S2). This hints that the residuals may be related to the specific geographical or environmental conditions.

To better understand the regional differences in the LCD distribution, we separately performed PCA using the data with low (inside the two sigma (ITS), $> -2\sigma$ and $< +2\sigma$, $n = 526$) and high (over the two sigma (OTS), $> +2\sigma$, $n = 30$) and under the two sigma (UTS, $< -2\sigma$, $n = 10$)

residuals (Fig. 7). For the ITS data, both C_{28} and $C_{28:1}$ 1,14-diols were closely loaded with nutrients on the PC1 (33.9% of the variance, Fig. 7a). However, for the OTS data, only the C_{28} 1,14-diol was closely loaded with nutrients on the PC1 (34.9% of the variance, Fig. 7b). This suggests that biological 1,14-diol producers in regions with the OTS data might be different than those with low residuals, primarily producing the C_{28} 1,14-diol under high nutrient conditions. Furthermore, we noted that the OTS samples were located mostly under the highly dissolved oxygen conditions of the bottom water (see Supplementary Fig. S2c). Such conditions would be favorable for the oxic degradation of the 1,15-diols than the 1,14-diols (Rodrigo-Gámiz et al., 2016), resulting in higher NDI-derived phosphate concentrations. For the UTS data, the C_{32} 1,15-diol was also positively loaded with nutrients and salinity on the PC1 (48.5% of the variance, Fig. 7c) along with the C_{28} 1,14-diol. This hints that the UTS sample sites, locating close to the coast (see Supplementary Fig. S2a), would have received riverine LCDs, which distorted the relationship between the LCDs and nutrients and resulted in lower NDI-derived phosphate concentrations. In such regions, reconstructing accurate nutrient conditions using the NDI might be further complicated due to different LCD producers and their different response sensitivity to nutrient conditions (e.g., de Bar et al., 2018).

We evaluated the relationship between nutrient concentrations and NDI values further by studying sinking particles at 1000 m water depth in the East Sea (Fig. 4). We excluded NDI data from the 2300 m water depth to eliminate the potential effect of lateral transport by resuspended sediments (e.g., Kim et al., 2009). The regression slope of the resulting calibration ($\text{NDI} = 1.134 \times [\text{PO}_4^{4-}] + 0.115$, $R^2 = 0.59$, $n = 26$, $p < 0.001$) was statistically different from the global surface sediment dataset (ANCOVA, $F_{(1,589)} = 128.55$, $p < 0.0001$) and the globally compiled SPM dataset ($\text{NDI} = 0.313 \times [\text{PO}_4^{4-}] + 0.020$, $R^2 = 0.76$, $n = 67$, $p < 0.001$; ANCOVA, $F_{(1,90)} = 140.7$, $p < 0.0001$). The higher regression slope for the sinking particles in the East Sea indicates a higher sensitivity of the C_{28} 1,14-diols producers to nutrient concentrations. Notably, the surface sediment samples from the East Sea were closely plotted with the sinking particle samples from the East Sea (see Fig. 4). The NDI-derived phosphate concentrations of SPM and surface sediments in the East Sea were in the range 0.71 – $1.03 \mu\text{M}$ using the new global calibration of the surface sediment dataset but much lower (0.16 – $0.28 \mu\text{M}$) using the local calibration (Table 1). Consequently, the phosphate concentrations derived from the local calibration fall better within the WOA13 annual mean phosphate concentration range (0.18 – $0.49 \mu\text{M}$).

In the East Sea, the total mass flux for the sampling period was dominated by biogenic opal, representing the diatom productivity (Kim



(caption on next column)

Fig. 7. PCA biplots of the fractional abundances of the LCDs and the environmental parameters for the (a) insides the two-sigma (ITS, $> -2\sigma$ and $< +2\sigma$, $n = 526$), (b) over the two-sigma (OTS, $> +2\sigma$, $n = 30$), and (c) under the two sigma (UTS, $< -2\sigma$, $n = 10$) data of the residual phosphate concentrations (i.e., NDI-derived - WOA13-derived phosphate concentrations) in Fig. 6. Black and red lines indicate the loading of the LCDs and the environmental factors, respectively. SST denotes sea surface temperature. (For interpretation of the references to colour in this figure legend, the reader is referred to the web version of this article.)

et al., 2017). Therefore, the total mass flux would seasonally co-vary with the NDI, reflecting the changes in nutrient concentration. However, the NDI values of sinking particles showed a different seasonality compared to the total mass fluxes (cf. Kim et al., 2017). Thus, the NDI values seem to be more dependent on nutrient conditions rather than marine primary production in the East Sea, which would also be influenced by other factors such as water temperature and water column stability. Nonetheless, the LCD distribution in the East Sea appears to differ from other oceanic settings, resulting in a steeper regression slope. To date, marine planktonic diatoms *Proboscia* and marine dictyochophyte algae *Apedinella radians* are known to produce the saturated C₂₈ 1,14-diols (Sinninghe Damsté et al., 2003; Rampen et al., 2007, 2009, 2011). However, the C_{28:1} 1,14-diol was not detected in *Apedinella radians* (Rampen et al., 2011). Considering that the C_{28:1} 1,14-diol was weakly loaded with nutrients than the C₂₈ 1,14-diol (see Fig. 5c), *Proboscia* diatoms may not be the only dominant 1,14-diol producers in the East Sea. Thus, the exact sources of the 1,14-diols still need to be determined in the East Sea.

5. Conclusion

In this study, we examined the temporal variation for individual LCD fluxes and the relationship between the LCDs and the environmental parameters such as nutrients, by analyzing sinking particles collected over a year from the East Sea. The fluxes of each 1,14-diol slightly differed from each other depending on seasons, implying that the seasonal variation in *Proboscia* communities would probably produce different types of the LCDs in the East Sea. The NDI at 1000 m water depth correlated well with the phosphate concentrations, suggesting that the production of the saturated and unsaturated C₂₈ 1,14-diols was influenced by the nutrient conditions in the East Sea. We also newly compiled the surface sediment dataset ($n = 566$) to assess the previous calibration between the NDI and phosphate in surface sediments ($n = 216$). Our results based on a newly compiled global surface sediment dataset confirmed that the NDI is a potential tool for reconstructing surface water phosphate conditions. However, the calibration based on the sinking particles at 1000 m water depth deviated from the newly compiled global surface sediment dataset. The local calibration predicted the phosphate concentrations in surface sediments in the East Sea better than the global calibration. Thus, our results indicate that in certain regional settings such as the East Sea, the 1,14-diol distribution may differ from other oceanic settings. This may be due to the presence of different 1,14-diol producers with different sensitivity responding to the nutrient conditions. Therefore, more studies on biological sources of the LCDs and their responses to nutrient conditions are required to better assess the NDI as a paleo-nutrient proxy. Studies should include additional analyses of SPM samples, sinking particles, and sediment cores from various oceanic settings.

Declaration of Competing Interest

None.

Acknowledgments

This study was supported by the project ‘Deep Water Circulation and

Material Cycling in the East Sea (0425-20170025) funded by the Ministry of Oceans and Fisheries (MOF), South Korea. This work was also supported by the National Research Foundation of Korea (NRF) grant funded by the Ministry of Science and ICT (MSIT) – South Korea (NRF-2015M1A5A1037243, KOPRI-PN20090).

Appendix A. Supplementary data

Supplementary data to this article can be found online at <https://doi.org/10.1016/j.marchem.2021.103937>.

References

- Balzano, S., Lattaud, J., Villanueva, L., Rampen, S.W., Brussaard, C.P.D., Van Bleijswijk, J., Bale, N., Sinninghe Damsté, J.S., Schouten, S., 2018. A quest for the biological sources of long chain alkyl diols in the western tropical North Atlantic Ocean. *Biogeosciences* 15, 5951–5968. <https://doi.org/10.5194/bg-15-5951-2018>.
- de Bar, M.W., Dorhout, D.J.C., Hopmans, E.C., Rampen, S.W., Sinninghe Damsté, J.S., Schouten, S., 2016. Constraints on the application of long chain diol proxies in the Iberian Atlantic margin. *Org. Geochem.* 101, 184–195. <https://doi.org/10.1016/j.orggeochem.2016.09.005>.
- de Bar, M.W., Stolwijk, D.J., McManus, J.F., Sinninghe Damsté, J.S., Schouten, S., 2018. A Late Quaternary climate record based on long chain diol proxies from the Chilean margin. *Clim. Past Discuss.* 1783–1803. <https://doi.org/10.5194/cp-2018-88>.
- de Bar, M.W., Weiss, G., Yildiz, C., Rampen, S.W., Lattaud, J., Bale, N.J., Mienis, F., Brummer, G.-J.A., Schulz, H., Rush, D., Kim, J.-H., Donner, B., Knies, J., Lückge, A., Stuut, J.-B.W., Sinninghe Damsté, J.S., Schouten, S., 2020. Global temperature calibration of the Long chain Diol Index in marine surface sediments. *Org. Geochem.* 142, 103983. <https://doi.org/10.1016/j.orggeochem.2020.103983>.
- Behrenfeld, M.J., Worthington, K., Sherrell, R.M., Chavez, F.P., Strutton, P., McPhaden, M., Shea, D.M., 2006. Controls on tropical Pacific Ocean productivity revealed through nutrient stress diagnostics. *Nature* 442, 1025–1028. <https://doi.org/10.1038/nature05083>.
- Gal, J.-K., Kim, J.-H., Nam, S.-I., Shin, K.-H., 2017. Effect of different GC columns on the quantitative analysis of long chain alkyl diols (LCDs). *Sea* 22, 45–55. <https://doi.org/10.7850/jkso.2017.22.2.045>.
- Gal, J.-K., Kim, J.-H., Shin, K.-H., 2018. Distribution of long chain alkyl diols along a south-north transect of the northwestern Pacific region: insights into a paleo sea surface nutrient proxy. *Org. Geochem.* 119, 80–90. <https://doi.org/10.1016/j.orggeochem.2018.01.010>.
- Gal, J.-K., Kim, J.-H., Kim, S., Lee, S.H., Yoo, K.-C., Shin, K.-H., 2019. Application of the newly developed nutrient diol index (NDI) as a sea surface nutrient proxy in the East Sea for the last 2400 years. *Quat. Int.* 503, 146–152. <https://doi.org/10.1016/j.quaint.2018.11.003>.
- García, H.E., Locarnini, R.A., Boyer, T.P., Antonov, J.I., Baranova, O.K., Zweng, M.M., Reagan, J.R., Johnson, D.R., 2013a. World Ocean Atlas 2013, Volume 4: Dissolved Inorganic Nutrients (phosphate, nitrate, silicate). In: NOAA Atlas NESDIS 4. Natl. Oceanogr. Data Cent. Intern. Rep., p. 25.
- Gelin, F., Boogers, I., Noordeeloo, A.A.M., Sinninghe Damsté, J.S., Rieglman, R., De Leeuw, J.W., 1997. Resistant biomacromolecules in marine microalgae of the classes Eustigmatophyceae and Chlorophyceae: geochemical implications. *Org. Geochem.* 26, 659–675. [https://doi.org/10.1016/S0146-6380\(97\)00035-1](https://doi.org/10.1016/S0146-6380(97)00035-1).
- Ichikawa, H., Beardsley, R.C., 2002. The current system in the Yellow and East China Seas. *J. Oceanogr.* 58, 77–99. <https://doi.org/10.1023/A:1015876701363>.
- Kang, Y.S., Choi, J.K., Eum, H.M., 2003. Ecological characteristics of phytoplankton communities in the coastal waters of Gori, Wolseong, Ulsan and Younggwang III. Distribution of dominant species and environmental variables. *Algae* 18, 29–47.
- Kang, Y.S., Choi, H.C., Lim, J.H., Jeon, I.S., Seo, J.H., 2005. Dynamics of the phytoplankton community in the coastal waters of Chuksan harbor, East Sea. *Algae* 20, 345–352.
- Kim, J.-H., Crosta, X., Michel, E., Schouten, S., Duprat, J., Sinninghe Damsté, J.S., 2009. Impact of lateral transport on organic proxies in the Southern Ocean. *Quat. Res.* 71, 246–250. <https://doi.org/10.1016/j.yqres.2008.10.005>.
- Kim, M., Hwang, J., Rho, T., Lee, T., Kang, D.-J., Chang, K.-I., Noh, S., Joo, H., Kwak, J. H., Kang, C.-K., Kim, K.-R., 2017. Biogeochemical properties of sinking particles in the southwestern part of the East Sea (Japan Sea). *J. Mar. Syst.* 167, 33–42. <https://doi.org/10.1016/j.jmarsys.2016.11.001>.
- Lattaud, J., Dorhout, D., Schulz, H., Castañeda, I.S., Sinninghe Damsté, J.S., Schouten, S., 2017a. The C₃₂ alkane-1,15-diol as a proxy of late quaternary riverine input in coastal margins. *Clim. Past Discuss.* 13, 1049–1061. <https://doi.org/10.5194/cp-2017-43>.
- Lattaud, J., Kim, J.-H., De Jonge, C., Zell, C., Sinninghe Damsté, J.S., Schouten, S., 2017b. The C₃₂ alkane-1,15-diol as a tracer for riverine input in coastal seas. *Geochim. Cosmochim. Acta* 202, 146–158. <https://doi.org/10.1016/j.gca.2016.12.030>.
- Lattaud, J., Kirkels, F., Peterse, F., Freymond, C.V., Eglinton, T.I., Hefter, J., Mollenhauer, G., Balzano, S., Villanueva, L., van der Meer, M.T.J., Hopmans, E.C., Sinninghe Damsté, J.S., Schouten, S., 2018. Long-chain diols in rivers: distribution and potential biological sources. *Biogeosci. Discuss.* 4147–4161. <https://doi.org/10.5194/bg-2018-116>.
- Lê, S., Josse, J., Husson, F., 2008. FactoMineR: an R package for multivariate analysis. *J. Stat. Softw.* <https://doi.org/10.18637/jss.v025.i01>.
- Lee, S.D., Yun, S.M., Park, J.S., Lee, J.H., 2015. Floristic survey of diatom in the three islands (Baeknyeong, Daecheong, Socheong) from yellow sea of Korea. *J. Ecol. Environ.* 38, 563–598. <https://doi.org/10.5141/ecoenv.2015.059>.
- Locarnini, R.A., Mishonov, A.V., Antonov, J.I., Boyer, T.P., Garcia, H.E., Baranova, O.K., Zweng, M.M., Paver, C.R., Reagan, J.R., Johnson, D.R., Hamilton, M., Seidov, D., 2013. In: Levitus, S. (Ed.), World Ocean Atlas 2013. Vol. 1: Temperature, NOAA Atlas NESDIS 73. A. Mishonov, Tech. Ed., p. 40. <https://doi.org/10.1182/blood-2011-06-357442>.
- Marchitto, T.M., 2013. Paleoclimatology, Physical and Chemical Proxies[Nutrient Proxies]. *Encyclopedia of Quaternary Science*, pp. 899–906. <https://doi.org/10.1016/B978-0-444-53643-3.00291-0>.
- Méjanelle, L., Sanchez-Gargallo, A., Bentaleb, I., Grimalt, J.O., 2003. Long chain n-alkyl diols, hydroxy ketones and sterols in a marine eustigmatophyte, *Nannochloropsis gaditana*, and in *Brachionus plicatilis* feeding on the algae. *Org. Geochem.* 34, 527–538. [https://doi.org/10.1016/S0146-6380\(02\)00246-2](https://doi.org/10.1016/S0146-6380(02)00246-2).
- Oksanen, J., Blanchet, F.G., Kindt, R., Legendre, P., Minchin, P.R., O'Hara, R.B., Simpson, G.L., Solymos, P., Stevens, M.H.H., Wagner, H., 2013. Package vegan: Community Ecology Package, R package version 2.3-1. <http://CRAN.R-project.org/package=vegan>.
- R Core team, 2015. R Core Team. R A Lang. Environ. Stat. Comput. R Found. Stat. Comput., Vienna, Austria. ISBN 3-900051-07-0. <http://www.R-project.org/>.
- Rampen, S.W., Schouten, S., Wakeham, S.G., Sinninghe Damsté, J.S., 2007. Seasonal and spatial variation in the sources and fluxes of long chain diols and mid-chain hydroxy methyl alkanolates in the Arabian Sea. *Org. Geochem.* 38, 165–179. <https://doi.org/10.1016/j.orggeochem.2006.10.008>.
- Rampen, S.W., Schouten, S., Koning, E., Brummer, G.J.A., Sinninghe Damsté, J.S., 2008. A 90 kyr upwelling record from the northwestern Indian Ocean using a novel long-chain diol index. *Earth Planet. Sci. Lett.* 276, 207–213. <https://doi.org/10.1016/j.epsl.2008.09.022>.
- Rampen, S.W., Schouten, S., Schefuß, E., Sinninghe Damsté, J.S., 2009. Impact of temperature on long chain diol and mid-chain hydroxy methyl alkanolates composition in *Proboscia* diatoms: results from culture and field studies. *Org. Geochem.* 40, 1124–1131. <https://doi.org/10.1016/j.orggeochem.2009.08.005>.
- Rampen, S.W., Schouten, S., Sinninghe Damsté, J.S., 2011. Occurrence of long chain 1,14-diols in *Apedinella radians*. *Org. Geochem.* 42, 572–574. <https://doi.org/10.1016/j.orggeochem.2011.03.009>.
- Rampen, S.W., Willmott, V., Kim, J.-H., Uliana, E., Mollenhauer, G., Schefuß, E., Sinninghe Damsté, J.S., Schouten, S., 2012. Long chain 1,13- and 1,15-diols as a potential proxy for palaeotemperature reconstruction. *Geochim. Cosmochim. Acta* 84, 204–216. <https://doi.org/10.1016/j.gca.2012.01.024>.
- Rodrigo-Gámiz, M., Rampen, S.W., Schouten, S., Sinninghe Damsté, J.S., 2016. The impact of oxid degradation on long chain alkyl diol distributions in Arabian Sea surface sediments. *Org. Geochem.* 100, 1–9. <https://doi.org/10.1016/j.orggeochem.2016.07.003>.
- Shimokawara, M., Nishimura, M., Matsuda, T., Akiyama, N., Kawai, T., 2010. Bound forms, compositional features, major sources and diagenesis of long chain, alkyl mid-chain diols in Lake Baikal sediments over the past 28,000 years. *Org. Geochem.* 41, 753–766. <https://doi.org/10.1016/j.orggeochem.2010.05.013>.
- Sinninghe Damsté, J.S., Rampen, S., Irene, W., Rijpstra, C., Abbas, B., Muyzer, G., Schouten, S., 2003. A diatomaceous origin for long-chain diols and mid-chain hydroxy methyl alkanolates widely occurring in quaternary marine sediments: indicators for high-nutrient conditions. *Geochim. Cosmochim. Acta* 67, 1339–1348. [https://doi.org/10.1016/S0016-7037\(02\)01225-5](https://doi.org/10.1016/S0016-7037(02)01225-5).
- Versteegh, G.J.M., Bosch, H.-J., De Leeuw, J.W., 1997. Potential palaeoenvironmental information of C₂₄ to C₃₆ mid-chain diols, keto-ols and mid-chain hydroxy fatty acids: a critical review. *Org. Geochem.* 27, 1–13. [https://doi.org/10.1016/S0146-6380\(97\)00063-6](https://doi.org/10.1016/S0146-6380(97)00063-6).
- Volkman, J.K., Barrett, S.M., Dunstan, G.A., Jeffrey, S.W., 1992. C₃₀–C₃₂ alkyl diols and unsaturated alcohols in microalgae of the class Eustigmatophyceae. *Org. Geochem.* 18, 131–138. [https://doi.org/10.1016/0146-6380\(92\)90150-V](https://doi.org/10.1016/0146-6380(92)90150-V).
- Yoon, Y.H., 2017. Spatio-temporal distributions of phytoplankton community in the coastal waters of central South Sea (CWoCSS), Korea. *J. Korea Acad. Coop. Soc.* 18, 441–453.
- Yun, S.M., Lee, J.H., 2011. Morphology and distribution of some marine diatoms, family Rhizosoleniaceae, genus *Proboscia*, *Neocalyptrella*, *Pseudosolenia*, *Guinardia*, and *Dacyliosolen* in Korean coastal waters. *Algae* 26, 299–315. <https://doi.org/10.4490/algae.2011.26.2.141>.
- Zweng, M.M., Reagan, J.R., Antonov, J.I., Mishonov, A.V., Boyer, T.P., Garcia, H.E., Baranova, O.K., Johnson, D.R., Seidov, D., Bidle, M.M., 2013. World Ocean Atlas 2013, Volume 2: Salinity. In: NOAA Atlas NESDIS 2, p. 39. <https://doi.org/10.1182/blood-2011-06-357442>.